Deep Sensing for Future Spectrum and Location Awareness 5G Communications

Bin Li, Shenghong Li, Arumugam Nallanathan, *Senior Member, IEEE*, and Chenglin Zhao

***Abstract*—Spectrum sensing based dynamic spectrum sharing is one of the key innovative techniques in future 5G communications. When realistic mobile scenarios are concerned, the location of primary user (PU) is of great significance to reliable spectrum detections and cognitive network enhancements. Given the dynamic disappearance of its emission signals, the passive locations tracking of PU, nevertheless, remains dramatically different from existing positioning problems. In this investigation, a new joint estimation paradigm, namely *deep sensing*, is proposed for such challenging spectrum and location awareness applications. A major advantage of this new sensing scheme is that the mutual interruption between the two unknown quantities is fully considered and, therefore, the PU's emission state is identified by estimating its moving positions jointly. Taking both PU's unknown states and its evolving positions into account, a unified mathematical model is formulated relying on a dynamic state-space approach. To implement the new sensing framework, a random finite set (RFS) based Bernoulli filtering algorithm is then suggested to recursively estimate unknown PU states accompanying its time-varying locations. Meanwhile, the sequential importance sampling is used to approximate intractable posterior densities numerically. Furthermore, an adaptive horizon expanding mechanism is specially designed to avoid the mis-tracking aroused by the intermittent disappearance of PU. Experimental simulations demonstrate that, even with mobile PUs, spectrum sensing can be realized effectively by tracking its locations incessantly. The location information, as an extra gift, may be utilized by cognitive performance optimizations.**

***Index Terms*—5G, dynamic spectrum sharing, deep sensing, PU localization, dynamic state-space model, recursive estimation.**

I. Introduction

With the capability of promoting spectral utilization by accessing licensed primary bands opportunistically, cognitive radios (CRs) based dynamic spectrum sharing is considered as a key feature of future 5G communications [1]. To implement CRs, spectrum sensing is one principal constituent for the intelligent mitigation of harmful inferences to primary user (PU) [2], [3], which aims to identify the bandwidth availability or PU's unknown emission states in real-time [4]–[6]. Given emerging CR applications (e.g., LTE-U and 802.11n), furthermore, the location information of PU may be of particular importance to both reliable spectrum sensing and enhancement of CR network performance [7]–[9]. A new spectrum sensing paradigm with the joint PU's locations estimation, therefore, would definitely provide a great promise to practical deployments of 5G communications, which has yet been rarely considered and remained still as a major challenge.

For the first task, i.e., spectrum sensing, various algorithms have been developed [2], [5], [6]. Traditional techniques, e.g., energy detector (ED) [10], matched filter (MF) detection [11] and cyclostationary feature detection [12], may in practice have different advantages and requirements [5]. Recent new sensing schemes include wavelet analysis [13], compressive sensing [14], covariance sensing [15] and probabilistic property-based sensing [16]. It is noteworthy that, by focusing on typical *non-mobile* CR applications (e.g., dynamic access of TV-bands) [17], unfortunately none of such methods have taken fully PU's dynamic positions into the sensing process. As far as the moving locations of PU are concerned, the received signals or observations will show remarkable fluctuations. Such a resulting special reception *uncertainty* in practice may easily make most existing schemes unattractive.

For the second task, i.e., location awareness, it should be noteworthy that the passive positioning of PU remains in sharp contrast to classical localization paradigms either of wireless sensor networks (WSNs) [18], or with externally aided systems (e.g., UWB or GPS) [19]. For the locations estimation in the context of dynamic spectrum access (DSA), there are following three challenges in the localization of PU. First, there is little information to be utilized, as a PU is endowed with the absolute priority on primary spectrum in which it is not bound to cooperate with secondary users (SUs). Thus, only the received signal strength (RSS) can be practically available during such passive location applications [20], while the time of arrival (ToA) information assumed by [21] may become impractical. Second, the PU's emission states will alter dynamically and, therefore, the received signals may be also disappeared intermittently, making the PU's position tracking even tougher. Third, in most instances, there may be no externally aided systems for typical CR networks.

The two tasks, in the considered spectrum sensing and location tracking scenario, may further become mutually interrelated. It may become even impossible to justify whether there contains PU's signals in current observation, let alone the inference or tracking of its moving positions in realistic CR applications. Most existing works, unfortunately, fail to consider such coupling influences, especially the tracking of PU's

Manuscript received August 11, 2014; revised December 6, 2014; accepted January 9, 2015. Date of publication May 6, 2015; date of current version June 22, 2015. This work was supported by Natural Science Foundation of China (NSFC) under Grants 61471061, and the Fundamental Research Funds for the Central Universities under Grant 2014RC0101.

B. Li and C. Zhao are with the School of Information and Communication Engineering (SICE), Beijing University of Posts and Telecommunications (BUPT), Beijing 100876, China (e-mail: stonebupt@gmail.com).

S. Li is with Department of Electronic Engineering, Shanghai Jiao Tong University, Shanghai 200240, China (e-mail: shli@stju.edu.cn).

A. Nallanathan is with the Department of Informatics, King's College London, London WC2 R2LS, U.K. (e-mail: nallanathan@ieee.org).

Color versions of one or more of the figures in this paper are available online at http://ieeexplore.ieee.org.

Digital Object Identifier 10.1109/JSAC.2015.2430279

dynamic locations under a silent state where it doesn't emit any electromagnetic signals [22]–[24]. For example, the Cramér-Rao bound of RSS-based PU positioning is investigated, which may be of theoretical significance, yet without considering the mutual interruption between sensing and localization [23]. The tracking of mobile PU, with a special emphasis on identifying malicious SUs in CR networks, is studied by [24], which, similarity, places little concerns on the important feature of CRs, i.e., detecting PU's states under the reception uncertainty and the reacting interruption on localization. To the best of our knowledge, joint spectrum sensing and positions tracking in the context of dynamic spectrum sharing (e.g., with PU's unknown emission states) has virtually not been reported in the open literature.

In this investigation, a promising deep sensing (DS) paradigm is designed for realistic spectrum and location awareness scenarios. To sum up, the main contributions of this work are the following four-folds.

1) The locations tracking of PU with unknown emission states is investigated, and a new DS framework is proposed, which estimates PU's locations at the same time of detecting its spectral occupancy. In particular, with this new scheme, the tracking of PU's positions will not be interrupted even when its emission has been suspended. Such a DS paradigm, therefore, is in contrast to either traditional sensing methods that ignores the mobile PU, or other positioning algorithms which fail to consider PU's dynamic emission states.
2) A novel mathematical formulation for spectrum sensing, relying on a dynamic state-space model (DSM) approach, is proposed to characterize the considered complex DS in the presence of mobile PUs. A distinct innovation of this new DSM, which may differentiate it from conventional sensing models or separate positioning models, is that the PU's unknown emission state is treated as another hidden state to be estimated, other than its varying positions. The mutual coupling relations, as a consequence, can be fully embodied. Given the limited information available in CR networks, the strength of summed-energy (i.e. RSS) is utilized to estimate the two hidden states recursively. It is noteworthy that such a DSM may be generalized to other scenes, e.g., the spectrum and location awareness application with time-varying fading propagations, which hence provides great promises to various different CR applications.
3) The major difficulty in solving the formulated DS problem, which may make existing sensing or localization algorithms invalid, is that either sensing or positioning procedure will easily become failure due to interruptions from the other one. The third contribution, accordingly, is that a flexible joint estimation algorithm is developed. The DS process, involving a PU's emission state and the other associated state (i.e., PU's unknown locations), is modeled as a Bernoulli random finite set (BRFS). Within the Bayesian inference framework, a recursive algorithm is then designed to estimate the PU's existence state accompanying its dynamic positions. The sequential importance sampling (SIS) technique is also adopted to approximate related posterior distributions numerically, which are in practice non-analytical and computationally intractable. To avoid the mis-tracking when a PU turns off, a horizon expanding mechanism is further integrated which will adaptively adjust the prior uncertainty of subsequent inference process. Consequently, the suggested scheme may realize joint spectrum sensing and location estimation effectively.
4) Both the performances of spectrum sensing and dynamic localization, with the moving PU of unknown emission states, are investigated. It is demonstrated by numerical experiments that, with estimated PU's locations, the reception uncertainty is calibrated and, therefore, the promising sensing performance is obtained even in realistic mobile scenarios. Meanwhile, the PU's location will be insistently tracked irrespective of its emission states, i.e., even it turns off. As an extra gift of sensing process, the recovered PU's locations will be utilized for further CR enhancement. The spectrum and location awareness DS scheme, which may be extended to other applications, puts an insight into spectrum sensing and will provide a brand-new idea of spectrum sharing in future 5G communications.

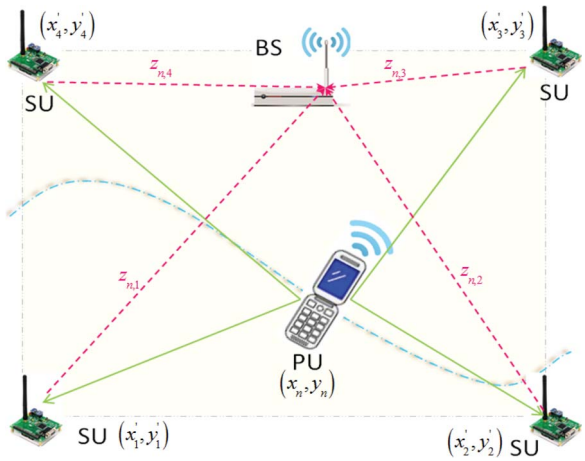

Fig. 1. A typical spectrum sensing scenario with $K = 4$ collaborative SUs and one random moving PU (e.g., a mobile terminal). The *green-solid* lines denote the 1st-phase sensing process, while the *red-dash* lines account for the 2nd-phase report process.

The rest of this article is structured as follows. In Section II, a DSM for joint spectrum sensing and PU's positioning is formulated. A Bayesian approach is then introduced in Section III, and a flexible algorithm is proposed, which is premised on RFS and would estimate PU's emission states and its locations jointly. A numerical approach is further suggested, which may implement Bayesian estimations effectively. Numerical experiments and performance evaluations are provided in Section IV. Finally, we conclude this investigation in Section V.

II. System Model

With the joint objective of spectrum sensing and PU localization, a cooperative scenario is concerned by this work, as illustrated by Fig. 1. For simplicity, K collaborative SU nodes are assumed to be located on a 2-D grid. The position of each

node, denoted by $\mathbf{b}_k = [x'_k, y'_k]^T$ $(k = 1, 2, \cdots, K)$, is known by a data center (maybe an access point or the base station). To realize spectrum sensing and locations tracking jointly, a two-stage scheme is used. In the 1st stage, the kth SU node will intercept nearby wireless environments at each discrete time n, and obtain a local observation $z_{n,k}$. In the 2nd stage, all SU nodes will report their observations toward to a data center. The data center will analyze the observation vector $\mathbf{z}_n = [z_{n,1}\ z_{n,2} \cdots z_{n,K}]^T$, and estimate the emission state of PU s_n accompanying its position (x_n, y_n).

A. DSM for Deep Sensing

In the consideration of more complex spectrum and location awareness scenario, a new DSM is established as follows.

$$s_n = S(s_{n-1}), \tag{1}$$

$$v_n = V(v_{n-1}, u_1), \tag{2}$$

$$\theta_n = \Theta(\theta_{n-1}, u_2), \tag{3}$$

$$\mathbf{l}_n = L(\mathbf{l}_{n-1}, v_n, \theta_n), \tag{4}$$

$$z_n = Z(\mathbf{l}_n, s_n, w_n(m)). \tag{5}$$

Here, eqs. (1)–(4) are referred to as *dynamic equations*, while eq. (5) accounts for the *measurement equation*.

1) The transitional function $S(\cdot): \mathbb{R}^1 \to \mathbb{R}^1$ specifies stochastic evolutions of PU's emission states $s_n \in \mathcal{S} = \{0, 1\}$ of the nth time as a 1st-order Markov process.
2) Two transitional functions $V(\cdot): \mathbb{R}^1 \to \mathbb{R}^1$ and $\Theta(\cdot): \mathbb{R}^1 \to \mathbb{R}^1$ describe two random behaviors of PU's movement speed v_n and orientation θ_n, which are driven independently by random noises u_1 and u_2, respectively.
3) Another transitional function $L(\cdot): \mathbb{R}^2 \to \mathbb{R}^2$ specifies the dynamics of PU's moving positions $\mathbf{l}_n = [x_n, y_n]^T$.
4) The observation function $Z(\cdot): \mathbb{R}^M \to \mathbb{R}^1$ gives the coupling relationship between two hidden states (i.e., s_n and l_n) and the measurement $z_{n,k} \in \mathcal{Z}(\mathcal{Z} \in \mathbb{R}^1)$.

For the ease of analysis, three assumptions are made to the established DSM model.

1) A common periodic sensing frame is adopted [5], [24], and the PU's emission state is assumed to be quasi-static. I.e., s_n will remain unchanged in one sensing duration T_s, but allowed to change among different durations.
2) The static Gaussian channel is considered. In this case, the observation $z_{n,k}$ is related only with the distance between the moving PU and the kth SU. The random measurement noise of the mth sample at the nth discrete time, denoted by $w_n(m)$, is further assumed to be the i.i.d. zero-mean additive white Gaussian noise (AWGN), with a variance of σ_w^2, which is independent of two hidden states.
3) The PU is assumed to be slowly moving. Its position $\mathbf{l}_n = [x_n, y_n]^T$, therefore, will remain invariant during each sensing duration T_s. That is, $\mathbf{l}_n$ is also independent of the sample index $m = 0, 1, \cdots, M-1$.

Next, we will elaborate on each equation.

B. Dynamics of PU State

It is shown that the evolution of PU's emission states over time can be modeled by a finite state machine $\mathcal{S} = \{S_0, S_1\}$, i.e., a two-state Markov transitional process [25]–[27]. If a PU is in the active emission state S_1 at the current sensing slot n, then it will stay in S_1 with a *survival* probability

$$p_s \triangleq \Pr\{s_{n+1} = 1 | s_n = 1\},$$

and jump into the sleep state S_0 with a probability $1 - p_s$ in the next time slot $n + 1$. If it is currently in the sleep state S_0, it will change to S_1 with a *birth* probability p_b:

$$p_b \triangleq \Pr\{s_{n+1} = 1 | s_n = 0\},$$

and then, may stay in S_0 in next slot with a probability of $1 - p_b$.

In practice, it is further assumed that the above probabilistic property is stationary, i.e., the dynamical transition is only related with specific wireless services, while keeping invariant for a given application in all the time (or at least, in a long period N). The statistical transitional probability matrix (TPM) of PU states may be defined as:

$$\boldsymbol{P} = \begin{bmatrix} (1 - p_b) & p_b, \\ (1 - p_s) & p_s. \end{bmatrix}. \tag{6}$$

C. Dynamic of PU's Positions

We firstly study the statistic behaviors of the speed and orientation of a moving PU. In this analysis, both of them are assumed to follow the *random walking* process. That is, given the moving speed v_{n-1} and orientation θ_{n-1} of the $(n-1)$th discrete time, then these two random variables at time n can be independently updated by:

$$v_n = v_{n-1} + u_1, \quad u_1 \sim \mathcal{N}\left(0, \sigma_v^2\right), \tag{7}$$

$$\theta_n = \theta_{n-1} + u_2, \quad u_2 \sim \mathcal{E}\left(0, \sigma_\theta^2\right), \tag{8}$$

where σ_v^2 and σ_θ^2 denote two variances of random PU's speed and orientation, respectively. It is noted that a Gaussian random noise, i.e., $\mathcal{N}(0, \sigma_v^2)$, and the other Laplace random noise, i.e., $\mathcal{E}(0, \sigma_\theta^2)$, are assumed as two driven terms of the random walking. The above *a priori* movement statistics are related with different PU's types (e.g., mobile human or vehicular) and operating scenarios (e.g., indoor or outdoor).

With the adaption equations of PU's speed and orientation θ_n, the dynamic evolution of its positions is specified by:

$$x_n = x_{n-1} + v_n \times cos(\theta_n), \tag{9}$$

$$y_n = y_{n-1} + v_n \times sin(\theta_n), \tag{10}$$

where x_n and y_n denote the horizon and vertical location axes of the PU at the nth discrete time.

D. Statistics of Observations

For realistic CR applications, the sensing observation based on summed-energy (i.e., RSS) is adopted in the analysis [5],

[10]. In practice, the sensing problem will be formulated as the following two-hypothesis problem, i.e.,

$$z_{n,k} \triangleq \sum_{m=1}^{M} \left[\gamma_k \sqrt{E_s} b_n(m) d_{n,k}^{-\alpha/2} \delta(s_n - S_1) + w_n(m)\right]^2 \quad (11a)$$

$$= \begin{cases} \sum_{m=1}^{M} w_n^2(m), & H_0, \\ \sum_{m=1}^{M} \left[\gamma_k \sqrt{E_s} b_n(m) d_{n,k}^{-\alpha/2} + w_n(m)\right]^2, & H_1, \end{cases} \quad (11b)$$

where $\delta(\cdot)$ denotes the Dirichlet function; $z_{n,k}$ is the RSS of the kth SU device; $d_{n,k}$ is the geographic distance between the kth SU and the moving PU at time n; α denotes the path-loss attenuation constant which is typically larger than 2; γ_k accounts for the receiving gain of the kth SU contributed by antennas or other processing; $M = T_s f_s$ denotes the samples size and f_s represents the sampling frequency. H_0 and H_1 correspond to two hypotheses, respectively, i.e., the absence and presence of PU's signals; $b_n(m)$ denote a sequence of PU's information symbols, with $m = 1, 2, \cdots, M$. For simplicity, the real-valued binary phase shift keying (BPSK) signal is assumed, e.g., $b_n(m) \in \mathcal{B} = \{+1, -1\}$, with an emission power of E_s.

As suggested, with a moving PU, the uncertainty in observations may become more obvious. From eq. (11), expect for PU's emission state (i.e., $s_n \in \mathcal{S}$), the observation is also related with unknown PU-SU distances

$$d_{n,k} \triangleq \|\mathbf{l}_n - \mathbf{b}_k\|_2 = \sqrt{\left(x_n - x_k'\right)^2 + \left(y_n - y_k'\right)^2}. \quad (12)$$

Conditioned on K distances $d_{n,k}$ and PU's emission state s_n, each component likelihood density, i.e., $p(z_{n,k}|d_{n,k}, s_n)$, then follows a central chi-square distribution with the degrees of freedom (DoF) of M under H_0, and a non-central chi-square distribution with M degrees under H_1.

As M is usually very large (e.g., $M \geqslant 100$), the likelihood functions in the data center may be approximated by Gaussian densities, based on an assumption of i.i.d. noise, i.e.,

$$p(\mathbf{z}_n|\mathbf{l}_n, s_n = 1) = \prod_{k=1}^{K} p(z_{n,k}|\mathbf{l}_n, s_n = 1), \quad (13a)$$

$$p(\mathbf{z}_n|\mathbf{l}_n, s_n = 0) = \prod_{k=1}^{K} p(z_{n,k}|s_n = 0). \quad (13b)$$

Alternatively, an equal gain combination (EGC) scheme may be also suggested in the data center, i.e., $Z_n \triangleq \sum_{k=1}^{K} z_{n,k}$. It is easily derived that the combined observation Z_n still follows a Gaussian distribution, i.e., $Z_n \sim \mathcal{N}(\mathsf{E}(Z_n|\mathbf{l}_n, s_n), \mathsf{V}(Z_n|\mathbf{l}_n, s_n))$, and its mean and variance, in the case of H_1, are respectively given by:

$$\mathsf{E}(Z_n|\mathbf{l}_n, s_n = 1) = \sum_{k=1}^{K} \mathsf{E}(z_{n,k}|\mathbf{l}_n, s_n = 1), \quad (14)$$

$$\mathsf{V}(Z_n|\mathbf{l}_n, s_n = 1) = \sum_{k=1}^{K} \mathsf{V}(z_{n,k}|\mathbf{l}_n, s_n = 1). \quad (15)$$

Similar forms can be ready for H_0. The involved means and variances are evaluated via:

$$\mathsf{E}(z_{n,k}|\mathbf{l}_n, S_1) = M \times \left(\sum_{k=1}^{K} \gamma_k^2 E_s d_{n,k}^{-\alpha} + K\sigma_w^2\right), \quad (16a)$$

$$\mathsf{V}(z_{n,k}|\mathbf{l}_n, S_1) = 4M \times \left(\sum_{k=1}^{K} \gamma_k^2 E_s d_{n,k}^{-\alpha} \sigma_w^2 + K\sigma_w^4\right), \quad (16b)$$

$$\mathsf{E}(z_{n,k}|S_0) = MK\sigma_w^2, \quad (16c)$$

$$\mathsf{V}(z_{n,k}|S_0) = 4MK\sigma_w^4. \quad (16d)$$

III. Deep Sensing

A. MAP Estimation of DS

Due to the inflexibility in dealing with joint position estimations, the classical *Neyman-Pearson* (NP) criterion may become less attractive to the considered DS scenario. This is mainly because, other than PU's unknown emission states, its moving positions need also to be estimated.

To perform this joint task, a Bayesian stochastic approach is designed for the formulated DS problem. Based on the established DSM, the maximum *a posteriori* (MAP) criterion is applied which would estimate the joint posterior PDF of two unknown states recursively, as in eq. (17), shown at the bottom of the page. Here, $s_{0:n} \triangleq \{s_0, s_1, \cdots, s_n\}$ denotes the trajectory of PU's emission states until the nth discrete time, $\mathbf{l}_{0:n}$ and $\mathbf{z}_{0:n}$ account for two trajectories of the varying positions and RSS observations, respectively. $\pi_{n|n-1}(\mathbf{l}_n|\mathbf{l}_{n-1})$ represents the prior transitional density of the moving positions $\mathbf{l}_n$. With the dynamic equations (7) and (8), the other two transitional densities in (17) are specified by:

$$p(v_n|v_{n-1}) \sim \mathcal{N}\left(v_n - v_{n-1}, \sigma_v^2\right),$$
$$p(\theta_n|\theta_{n-1}) \sim \mathcal{E}\left(\theta_n - \theta_{n-1}, \sigma_\theta^2\right).$$

For clarity, we further denote the two hidden states by one state vector, i.e., $\mathbf{S}_n \triangleq \{s_n, \mathbf{l}_n\}$. As an effective tool to derive the estimations of hidden states, the well-known two-step algorithm, i.e., first predict and then update, can be suggested, which may theoretically acquire the optimal posterior distribution of $\mathbf{S}_n$ in a recursive manner.

$$(\hat{\mathbf{l}}_n, \hat{s}_n) = \arg \max_{\mathbf{l}_n \in \mathbb{R}^2, s_n \in \mathcal{S}} p(\mathbf{l}_{0:n}, s_{0:n}|\mathbf{z}_{0:n}) \left|\pi_{n|n-1}(\mathbf{l}_n|\mathbf{l}_{n-1}), p(v_n|v_{n-1}), p(\theta_n|\theta_{n-1}), p(s_n|s_{n-1})\right. \quad (17)$$

1) Predict Stage: Let $p_{n-1|n-1}(\mathbf{S}_{n-1}|\mathbf{z}_{1:n-1})$ denotes the posterior density at time $n-1$. Given the assumed 1st-order Markov chain and *a priori* distribution of $\mathbf{S}_0$, i.e., $p(\mathbf{S}_0)$, the 1st-step prediction $p_{n|n-1}(\mathbf{S}_n|\mathbf{z}_{1:n-1})$ may be obtained:

$$p_{n|n-1}(\mathbf{S}_n|\mathbf{z}_{1:n-1}) = \int \phi_{n|n-1}(\mathbf{S}_n|\mathbf{S}_{1:n-1}) p_{n-1|n-1}(\mathbf{S}_{n-1}|\mathbf{z}_{1:n-1}) d\mathbf{S}_{n-1}, \quad (18)$$

where the traditional density $\phi_{n|n-1}(\mathbf{S}_n|\mathbf{S}_{1:n-1})$ is given by:

$$\phi_{n|n-1}(\mathbf{S}_n|\mathbf{S}_{1:n-1}) = \phi_{n|n-1}(\mathbf{S}_n|\mathbf{S}_{n-1}) \overset{(a)}{=} p(s_n|s_{n-1}) \times \pi_{n|n-1}(\mathbf{l}_n|\mathbf{l}_{n-1}).$$

Here, (a) holds for the independent evolutions between PU's emission states and its locations.

2) Update Stage: To refine the inaccurate predicted density derived only from *a priori* knowledge, new measurements $\mathbf{z}_n$ accompanying the likelihood density $\varphi_n(\mathbf{z}_n|\mathbf{S}_n)$ would be utilized. Thus, the Bays update is applied, i.e.,

$$p_{n|n}(\mathbf{S}_n|\mathbf{z}_{1:n}) = \frac{\varphi_n(\mathbf{z}_n|\mathbf{S}_n) p_{n|n-1}(\mathbf{S}_n|\mathbf{z}_{1:n-1})}{\int \varphi_n(\mathbf{z}_n|\mathbf{S}_n) p_{n|n-1}(\mathbf{S}_n|\mathbf{z}_{1:n-1}) d\mathbf{S}_n}. \quad (19)$$

With the above predict-and-update propagation, the target joint density $p_{n|n}(\mathbf{S}_n|\mathbf{z}_{1:n})$ may be estimated recursively.

The classical sequential estimation framework, unfortunately, may become infeasible for the DS process which takes PU's varying positions. First, note from eq. (11), the dynamic distance $d_{n,k}$ may disappear completely from the energy observation $z_{n,k}$, when a PU turns *off* (i.e., H_0 or $s_n = S_0$). Let alone the Bayesian inference of unknown positions, the related likelihood involving PU-SU distances may be unavailable in such a case, making the tracking of PU's dynamic locations very tough. Second, without a deterministic PU's position, the estimation of PU states will become inaccurate due to the resulting reception uncertainty (especially for energy-based sensing method, e.g., ED). Third, even if the likelihood function could be utilized when a PU is *on* (i.e., H_1 or $s_n = S_1$), the involved marginal integration seems still to be analytically intractable and computationally prohibitive to many practical uses.

B. Bernoulli Random Finite States

The dynamic appearance (or disappearance) of PU's signals is used to be treated directly as another *separate* random state (i.e., s_n) [3], [5], [6], [26], [27], other than the PU's dynamic position (i.e., $\mathbf{l}_n$). As mentioned, such a traditional simple and intuitive formulation, however, will lead to great difficulties in joint estimations. In this investigation, from a more attractive perspective, the whole dynamic behaviors of two hidden states are structured into one unified random process $\boldsymbol{\mathcal{F}}$, which is referred to as RFS [28].

1) Cardinality of RFS: The RFS may be considered, in essence, as a special stochastic set whose elements (including the number of elements) will be changed randomly [29]. In contrast to classical random vectors, now the cardinality (i.e., the number of elements) of the RFS $\boldsymbol{\mathcal{F}}$, which is denoted by $c = |\boldsymbol{\mathcal{F}}|$, also becomes a random process. Apart from the c-element joint distribution $p(F_1, \cdots, F_c)$, $\{F_1, \cdots, F_c\} \in \mathbb{R}^c$, a cardinality distribution $\kappa(c) = \Pr\{|\boldsymbol{\mathcal{F}}| = c\} (c \in \mathbb{N}_0)$ is particularly specified to characterize an RFS.

Given the considered spectrum sensing scene with one mobile PU,[1] we will have either $\boldsymbol{\mathcal{F}}_n = \{\mathbf{l}_n \in \mathbb{R}^2\}$ or $\boldsymbol{\mathcal{F}}_n = \varnothing$, i.e., $c = 1$ and $|\boldsymbol{\mathcal{F}}_n| \in \{0, 1\}$. Accordingly, one binary *existence* variable λ_n is used to token the random appearance or disappearance of PU signals. If a PU emits signals (i.e., H_1) at time n, then we have $\lambda_n = 1$ and otherwise, $\lambda_n = 0$ (i.e., S_0 or H_0). Obviously, λ_n is a random Bernoulli variable, which may either be empty (with probability $1-q$) or have a single element (with probability q). Thus, the random cardinality of such a Bernoulli RFS is

$$\kappa(c) = \begin{cases} 1-q & \text{if } \boldsymbol{\mathcal{F}}_n = \varnothing \text{ or } \lambda_n = 0, \quad (20a) \\ q & \text{if } \boldsymbol{\mathcal{F}}_n = \{\mathbf{l}_n\} \text{ or } \lambda_n = 1. \quad (20b) \end{cases}$$

2) PDF of RFS: According to the Mahler's theorem [28], [29], the finite set statistics (FISST) PDF denoted by $p(\boldsymbol{\mathcal{F}}_n)$, may be conveniently employed to describe the probabilistic behaviors of an RFS, like other traditional random variables, i.e.,

$$p(\boldsymbol{\mathcal{F}}_n = \{F_1, \cdots, F_c\}) = c! \kappa(c) p(F_1, \cdots, F_c). \quad (21)$$

With the set integration $\int p(\boldsymbol{\mathcal{F}}_n) \delta \boldsymbol{\mathcal{F}}_n$ on $\boldsymbol{\mathcal{F}}_n$ (rather than the marginalization as in a common random variable), it is seen that $p(\boldsymbol{\mathcal{F}}_n)$ can be indeed used as a PDF, i.e.,

$$\int_{\boldsymbol{\mathcal{F}}_n} p(\boldsymbol{\mathcal{F}}_n) \delta \boldsymbol{\mathcal{F}} = p(\varnothing) + \sum_{c=1}^{\infty} \frac{1}{c!} \int_{\{F_1, \cdots, F_c\} \in \mathbb{R}^c} p(F_1, \cdots, F_c) dF_1 \cdots dF_c \equiv 1.$$

In the presence of a realistic mobile PU, the singleton state associate with the PU's appearance (i.e., $|\boldsymbol{\mathcal{F}}_n| = 1$) corresponds actually to its dynamic positions $\mathbf{l}_n$. With the cardinality distribution $\kappa(c)$ and the state distribution PDF $p(\mathbf{l}_n)$, the FISST PDF is simplified to:

$$p(\boldsymbol{\mathcal{F}}_n) = \begin{cases} 1-q & \text{if } \boldsymbol{\mathcal{F}}_n = \varnothing, \quad (22a) \\ q \times p(\alpha) & \text{if } \boldsymbol{\mathcal{F}}_n = \{\mathbf{l}_n\}. \quad (22b) \end{cases}$$

Note that, for the special case where the cardinality c is larger than 1, we will have $p(\boldsymbol{\mathcal{F}}_n) = 0$.

3) Dynamic Transitions of RFS: Based on the new DSM, the dynamic transitional behaviors of Bernoulli RSF $\boldsymbol{\mathcal{F}}_n$ also follow a 1st-order Markov process. That is, for two possible cardinalities at the time $(n-1)$, the prior transitional probabilities will be determined by:

$$\phi_{n|n-1}(\boldsymbol{\mathcal{F}}_n|\varnothing) = \begin{cases} 1-p_b & \text{if } \boldsymbol{\mathcal{F}}_n = \varnothing, \quad (23a) \\ p_b b_{n|n-1}(\mathbf{l}_n) & \text{if } \boldsymbol{\mathcal{F}}_n = \{\mathbf{l}_n\}, \quad (23b) \end{cases}$$

[1] In this analysis, we consider only one single PU to be detected and tracked. The generalization to multiple PUs is straightforward.

and

$$\phi_{n|n-1}(\boldsymbol{\mathcal{F}}_n|\{\mathbf{l}_n\}) = \begin{cases} 1-p_s & \text{if } \boldsymbol{\mathcal{F}}_n = \varnothing, \quad (24a) \\ p_s \pi_{n|n-1}(\mathbf{l}_n|\mathbf{l}_{n-1}) & \text{if } \boldsymbol{\mathcal{F}}_n = \{\alpha_n\}, \quad (24b) \end{cases}$$

respectively, where $b_{n|n-1}(\mathbf{l}_n)$ refers to as the birth density, which accounts for the initial density of a singleton state $\{\mathbf{l}_n\}$ when the PU object is *re-activated* or re-emitting, i.e., $p(\mathbf{l}_n|q_{n-1|n-1}=0)$ [30]. The birth density should be designed properly to achieve good performance, which will be discussed in subsequent Section III-E. Based on eqs. (7)–(8), the transitional density of PU's dynamic locations, i.e., $\pi_{n|n-1}(\mathbf{l}_n|\mathbf{l}_{n-1})$, is given by:

$$\pi_{n|n-1}(\mathbf{l}_n|\mathbf{l}_{n-1}) = \frac{1}{\sqrt{2\pi}\sigma_v} exp\left\{-\frac{(\|\mathbf{l}_n - \mathbf{l}_{n-1}\|_2 - v_{n-1})^2}{2\sigma_v^2}\right\} \times \frac{1}{2\sigma_\theta^2} exp\left[-\frac{|\mathtt{ang}(\mathbf{l}_n - \mathbf{l}_{n-1}) - \theta_{n-1}|}{\sigma_\theta^2}\right], \quad (25)$$

where $\mathtt{ang}(\cdot)$ denote the angle of a displacement vector, i.e., $\mathtt{ang}(\mathbf{l}_n - \mathbf{l}_{n-1}) = \tan^{-1}\left(\frac{y_n - y_{n-1}}{x_n - x_{n-1}}\right)$.

With the RSS observations $\mathbf{z}_n$, the likelihood distribution, denoted by $\varphi(\mathbf{z}_n|\mathbf{l}_n)$, is easily derived, i.e.,

$$\varphi(\mathbf{z}_n|\boldsymbol{\mathcal{F}}_n) = \begin{cases} \mathcal{N}\{\mathsf{E}(\mathbf{z}_n|\mathbf{l}_n, s_n=1), \mathsf{V}(\mathbf{z}_n|\mathbf{l}_n, s_n=1)\} \\ \qquad\qquad \text{if } \boldsymbol{\mathcal{F}}_n = \{\mathbf{l}_n\}, \quad (26a) \\ \mathcal{N}\{\mathsf{E}(\mathbf{z}_n|s_n=0), \mathsf{V}(\mathbf{z}_n|s_n=0)\} \\ \qquad\qquad \text{if } \boldsymbol{\mathcal{F}}_n = \varnothing. \quad (26b) \end{cases}$$

4) Estimations of RFS: For the formulated RFS $\boldsymbol{\mathcal{F}}_n$, once two related distributions, i.e., the posterior density of PU's appearance and *a posteriori* spatial PDF of moving locations $\boldsymbol{\mathcal{F}}_n = \{\mathbf{l}_n\}$, are determined, then we may easily obtain the FISST PDF $p_{n|n}(\boldsymbol{\mathcal{F}}_n|\mathbf{z}_{1:n})$ [31].

More specifically, the posterior density of the PU's appearance is denoted by:

$$q_{n|n} \triangleq \Pr\{\boldsymbol{\mathcal{F}}_n = \{\mathbf{l}_n\}|\mathbf{z}_{1:n}\}, \quad (27)$$

and *a posteriori* spatial PDF of $\boldsymbol{\mathcal{F}}_n = \{\mathbf{l}_n\}$, i.e.,

$$f_{n|n}(\boldsymbol{\mathcal{F}}_n = \{\mathbf{l}_n\}) \triangleq p(\mathbf{l}_n|\mathbf{z}_{1:n}). \quad (28)$$

C. RFS Estimation With Sequential MAP

Rather than estimating two hidden states separately as in the previous works [26], [34], RFS will deal with one unified random variable $\boldsymbol{\mathcal{F}}_n$, which, however, will tune *on-off* dynamically. With the new RFS framework, therefore, two hidden states need not to be derived independently. By casting the stochastic DS problem into an RFS which may effectively handle the coupling interruption between PU's positions and its emission states, the PU's dynamic states can be then estimated jointly via the Bernoulli random cardinality. So, the first two problems in designing DS algorithms may be addressed.

A generalized two-stage recursive framework may be applied, even for the established RFS. However, notice that a major difference between the generalized propagation of RFS and traditional sequential estimation (i.e., eqs. (18), (19)) is that, rather than the distribution marginalization, the set integration (i.e., $\delta\boldsymbol{\mathcal{F}}_n$) will be used in RFS, i.e.,

$$p_{n|n-1}(\boldsymbol{\mathcal{F}}_n|\mathbf{z}_{1:n-1}) = \int_{\boldsymbol{\mathcal{F}}_n} \phi_{n|n-1}(\boldsymbol{\mathcal{F}}_n|\boldsymbol{\mathcal{F}}_{1:n-1}) p_{n-1|n-1} \times (\boldsymbol{\mathcal{F}}_{n-1}|\mathbf{z}_{1:n-1}) \delta\boldsymbol{\mathcal{F}}_{n-1},$$

$$p_{n|n}(\boldsymbol{\mathcal{F}}_n|\mathbf{z}_{1:n}) = \frac{\varphi_n(\mathbf{z}_n|\boldsymbol{\mathcal{F}}_n) p_{n|n-1}(\boldsymbol{\mathcal{F}}_n|\mathbf{z}_{1:n-1})}{\int_{\boldsymbol{\mathcal{F}}_n} \varphi_n(\mathbf{z}_n|\boldsymbol{\mathcal{F}}_n) p_{n|n-1}(\boldsymbol{\mathcal{F}}_n|\mathbf{z}_{1:n-1}) \delta\boldsymbol{\mathcal{F}}_n}.$$

Most existing schemes, unfortunately, fail to address RFS estimations under a sequential MAP criterion [2], [5], [26]. To solve the above *generalized* Bayesian inference and thereby derive the estimation of Bernoulli RFS $\boldsymbol{\mathcal{F}}_n$, a particular stochastic algorithm should be designed, with which the posterior PDFs of RFS would be recursively estimated based on the formulated DSM and measurements $\mathbf{z}_{1:n}$.

D. Bernoulli Filtering for BRFS

Much similar to traditional Bayesian prediction-update process, the two posterior densities, i.e., $p_{n|n}(\boldsymbol{\mathcal{F}}_n|\mathbf{z}_{1:n})$ and $f_{n|n}(\boldsymbol{\mathcal{F}}_n)$, will be propagated recursively.

1) Prediction Stage: With the prior transitional property, the 1-step predicting densities of the two terms, i.e., $q_{n|n-1}$ and $f_{n|n-1}(\mathbf{l}_n)$, will be derived from the 1st-order transitions. Based on the above analysis, the predicted posterior FISST PDF at time n is easily expanded to:

$$\begin{aligned} &p_{n|n-1}(\boldsymbol{\mathcal{F}}_n|\mathbf{z}_{1:n-1}) \\ &= \int_{\boldsymbol{\mathcal{F}}_n} \phi_{n|n-1}(\boldsymbol{\mathcal{F}}_n|\boldsymbol{\mathcal{F}}_{n-1}) p_{n-1|n-1}(\boldsymbol{\mathcal{F}}_{n-1}|\mathbf{z}_{1:n-1}) \delta\boldsymbol{\mathcal{F}}_{n-1} \\ &= \phi_{n|n-1}(\boldsymbol{\mathcal{F}}_n|\varnothing) p_{n-1|n-1}(\varnothing|\mathbf{z}_{1:n-1}) \\ &\quad + \int \phi_{n|n-1}(\boldsymbol{\mathcal{F}}_n|\mathbf{l}_{n-1}) p_{n-1|n-1}(\mathbf{l}_{n-1}|\mathbf{z}_{1:n-1}) d\mathbf{l}_{n-1}. \quad (29) \end{aligned}$$

Considering the first case $\boldsymbol{\mathcal{F}}_n = \varnothing$ (i.e., the PU turns off) and the underlying relation $p_{n|n-1}(\varnothing|\mathbf{z}_{1:n-1}) = 1 - q_{n|n-1}$, the predicted posterior FISST PDF will be easily derived via some manipulations on (29), i.e.,

$$\begin{aligned} q_{n|n-1} &= 1 - \left[(1-p_b) \times (1-q_{n-1|n-1}) + (1-p_s) \times q_{n-1|n-1}\right] \\ &= p_b \times (1-q_{n-1|n-1}) + p_s \times q_{n-1|n-1}. \quad (30) \end{aligned}$$

Checking the other case $\boldsymbol{\mathcal{F}}_n = \{\mathbf{l}_n\}$ (i.e., the PU turns on), we may derived the predicted posterior FISST as in (31), by similarly utilizing the relationship $p_{n|n-1}(\{\mathbf{l}_n\}|\mathbf{z}_{1:n-1}) = q_{n|n-1} \times f_{n|n-1}(\mathbf{l}_n)$.

$$f_{n|n-1}(\mathbf{l}_n) = \frac{p_b(1-q_{n-1|n-1}) b_{n|n-1}(\mathbf{l}_n)}{q_{n|n-1}} + \frac{p_s q_{n-1|n-1} \times \int \pi_{n-1|n-1}(\mathbf{l}_n|\mathbf{l}_{n-1}) f_{n-1|n-1}(\mathbf{l}_{n-1}) d\mathbf{l}_{n-1}}{q_{n|n-1}}. \quad (31)$$

It is seen that, from the physical implications of eq. (30) and (31), both the predicted density $q_{n|n-1}$ and the spatial density $f_{n|n-1}(\mathbf{l}_n)$ may involve two components, i.e., the birth component of a new PU and the survival component of an already existed PU. 1) The first birth term is specified basically by the transition or switch of a *disappeared* PU (i.e., p_b); and 2) the second survival one is contributed essentially by the *continuation* of an appeared PU (i.e., p_s).

2) Update Stage: According to different PU's emission states, two cases will be studied separately. For the first case $\boldsymbol{\mathcal{F}}_n = \varnothing$, the update equation is given by:

$$p_{n|n}(\varnothing|\mathbf{z}_{1:n}) = \varphi_n(\mathbf{z}_n|\varnothing)p_{n|n-1}(\varnothing|\mathbf{z}_{1:n-1})/p(\mathbf{z}_n|\mathbf{z}_{1:n-1}).$$

Based on the set integration operation, the prediction term in the denominator tends to:

$$\begin{aligned} p(\mathbf{z}_n|\mathbf{z}_{1:n-1}) &= \int_{\boldsymbol{\mathcal{F}}_n} \varphi_n(\mathbf{z}_n|\boldsymbol{\mathcal{F}}_n)p_{n|n-1}(\boldsymbol{\mathcal{F}}_n|\mathbf{z}_{1:n-1})\delta\boldsymbol{\mathcal{F}}_n \\ &= \varphi_n(\mathbf{z}_n|\varnothing)p_{n|n-1}(\varnothing|\mathbf{z}_{1:n-1}) \\ &\quad + \int \varphi_n(\mathbf{z}_n|\mathbf{l}_n)p_{n|n-1}(\mathbf{l}_n|\mathbf{z}_{1:n-1})d\mathbf{l}_n. \end{aligned} \tag{32}$$

Replacing the underlying identical relations $p_{n|n-1}(\varnothing|\mathbf{z}_{1:n-1}) = 1 - q_{n|n-1}$ and $p_{n|n-1}(\mathbf{l}_n|\mathbf{z}_{1:n-1}) = q_{n|n-1} \times f_{n|n-1}(\mathbf{l}_n)$ into eq. (32), we obtain

$$\begin{aligned} p(\mathbf{z}_n|\mathbf{z}_{1:n-1}) &= (1 - q_{n|n-1})\varphi_n(\mathbf{z}_n|\varnothing) \\ &\quad + q_{n|n-1}\int \varphi_n(\mathbf{z}_n|\mathbf{l}_n)f_{n|n-1}(\mathbf{l}_n)d\mathbf{l}_n. \end{aligned} \tag{33}$$

Further checking the updating equation, then the recursive refinement of the posterior existence density $q_{n|n}$ is derived by:

$$q_{n|n} = \frac{q_{n|n-1}\int r_n(\mathbf{z}_n|\mathbf{l}_n)f_{n|n-1}(\mathbf{l}_n)d\mathbf{l}_n}{(1 - q_{n|n-1}) + q_{n|n-1}\int r_n(\mathbf{z}_n|\mathbf{l}_n)f_{n|n-1}(\mathbf{l}_n)d\mathbf{l}_n}, \tag{34}$$

where $r_n(\mathbf{z}_n|\mathbf{l}_n)$ accounts for the likelihoods ratio between two hypothesis under the current measurement $\mathbf{z}_n$, i.e.,

$$r_n(\mathbf{z}_n|\mathbf{l}_n) \triangleq \varphi_n(\mathbf{z}_n|\mathbf{l}_n)/\varphi_n(\mathbf{z}_n|\varnothing). \tag{35}$$

For the second case $\boldsymbol{\mathcal{F}}_n = \{\mathbf{l}_n\}$, the underlying constraint $p_{n|n}(\mathbf{l}_n|\mathbf{z}_{1:n}) = q_{n|n} \times f_{n|n}(\mathbf{l}_n)$ may be applied similarly. By further interpreting the analytical form of updated density $q_{n|n}$, the recursive update of the spatial PDFs will be finally obtained from:

$$f_{n|n}(\mathbf{l}_n) = \frac{r_n(\mathbf{z}_n|\mathbf{l}_n)f_{n|n-1}(\mathbf{l}_n)}{\int r_n(\mathbf{z}_n|\mathbf{l}_n)f_{n|n-1}(\mathbf{l}_n)d\mathbf{l}_n}. \tag{36}$$

With the above generalized two-stage propagation, the joint estimation of two posterior densities, i.e., the probability of existence $q_{n|n}$ and the spatial PDF $f_{n|n}(\mathbf{l}_n)$, would be derived. Combined with two predict parts, i.e., $q_{n|n-1}$ and $f_{n|n-1}(\mathbf{l}_n)$, then the Bernoulli RFS $\boldsymbol{\mathcal{F}}_n$ may be estimated recursively.

Note from the above analysis, despite a single RFS $\boldsymbol{\mathcal{F}}_n$, the appearance of PU's emission signal (i.e., $q_{n|n}$) will be estimated jointly with its positions (i.e., $\mathbf{l}_n$). The presented scheme is thereby different from other existing techniques [26], [27], in which two hidden states are treated as two separate quantities and are estimated independently. Except for the generality and effectiveness, the new scheme, within the unified DS paradigm, may obtain attractive sensing and tracking performance by jointly acquiring two hidden states.

E. Implementation of Bernoulli Filtering

It should be emphasized that the estimation of PU's locations may involve the marginalization on the continuous distribution, e.g., the predict density $f_{n|n-1}(\mathbf{l}_n)$ in eqs. (31), which may be computationally intractable. To cope with this problem, the SIS based numerical approximation approach is suggested alternatively for the considered problem, which may also realize the Bayesian inference.

1) Particle Filtering: Based on the simulated Monte-carlo method, PF manages to approximate complex realistic distributions via a group of random discrete measures (i.e., particles) $\mathbf{x}_{n|n-1}^{(i)}$ with evolving probability masses (or weights) $w_{n|n-1}^{(i)}(i = 1, 2, \cdots, I)$ [32].

To be specific, a proposal density $\rho(\mathbf{x}_{n|n-1}|\mathbf{x}_{1:n-1}^{(i)}, \mathbf{z}_{1:n-1})$, which is related with the target posterior density $f_{n|n-1}(\mathbf{x})$, will be specified firstly, from which total I discrete simulated particles will be drawn, i.e., $\mathbf{x}_{n|n-1}^{(i)} \sim \rho(\mathbf{x}_{n|n-1}|\mathbf{x}_{1:n-1}^{(i)}, \mathbf{z}_{1:n-1})$. Subsequently, with discrete particles measures, the target distribution $f_{n|n-1}(\mathbf{x})$ would be approximated numerically via $\hat{f}_{n|n-1}(\mathbf{x}) \simeq \sum_{i=1}^{I} w_{n|n-1}^{(i)}\delta(\mathbf{x} - \mathbf{x}_{n|n-1}^{(i)})$, where the associated importance weight $w_{n|n-1}^{(i)}$ are updated recursively by:

$$w_{n|n-1}^{(i)} = w_{n-1|n-1}^{(i)} \frac{p\left(\mathbf{z}_n \middle| \mathbf{x}_{n|n-1}^{(i)}\right) p\left(\mathbf{x}_{n|n-1}^{(i)} \middle| \mathbf{x}_{n-1|n-1}^{(i)}\right)}{\rho\left(\mathbf{x}_{n|n-1} \middle| \mathbf{x}_{1:n-1}^{(i)}, \mathbf{z}_{1:n-1}\right)}. \tag{37}$$

2) Bernoulli BF: For the formulated Bernoulli RFS, a Bernoulli PF (BPF) is suggested to approximate the predicted density, i.e., $f_{n|n-1}(\mathbf{x})$. As seen from eq. (31), $f_{n|n-1}(\mathbf{x})$ actually involves two components. Thus, a *piece-wise* proposal distribution is employed to simulate discrete particles, i.e.,

$$\mathbf{x}_{n|n-1}^{(i)} = \begin{cases} \beta(\mathbf{x}_{n|n-1}|\mathbf{z}_{1:n-1}), \\ \qquad i = I - B + 1, \cdots, I, & \text{(38a)} \\ \xi\left(\mathbf{x}_{n|n-1} \middle| \mathbf{x}_{1:n-1}^{(i)}, \mathbf{z}_{1:n-1}\right), \\ \qquad i = 1, 2, \cdots, I - B. & \text{(38b)} \end{cases}$$

In the above proposal distribution, the first B particles are used to approximate the first term in eq. (31), while the following $(I - B)$ particles are used to evaluate the second term. With these discrete random particles, according to eq. (37), the associative weights will be updated by:

$$w_{n|n-1}^{(i)} = \begin{cases} \frac{p_b(1-q_{n-1|n-1})}{q_{n|n-1}} \frac{b_{n|n-1}(\mathbf{x}_{n|n-1})}{B \times \beta(\mathbf{x}_{n|n-1}|\mathbf{z}_{1:n-1})}, \\ \qquad i = I - B + 1, \cdots, I, & \text{(39a)} \\ \frac{p_s q_{n-1|n-1}}{q_{n|n-1}} \frac{\pi_{n|n-1}\left(\mathbf{x}_{n|n-1}^{(i)} \middle| \mathbf{x}_{n-1}^{(i)}\right)}{\xi\left(\mathbf{x}_{n|n-1} \middle| \mathbf{x}_{1:n-1}^{(i)}, \mathbf{z}_{1:n-1}\right)} w_{n-1|n-1}^{(i)}, \\ \qquad i = 1, 2, \cdots, I - B. & \text{(39b)} \end{cases}$$

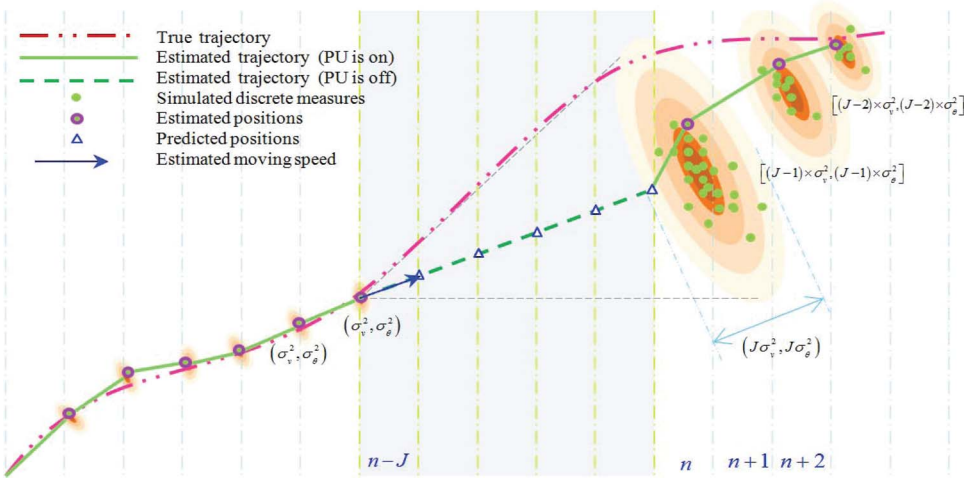

Fig. 2. Illustrations of the designed AHE process and the dynamic tracking process of realistic PU's locations. The PU will stay in the silence state (i.e., H_0 or $\mathcal{S}_0$) in discrete times of $[n-J, \cdots, n-1]$, and then enter into the emission state (i.e., H_1 or $\mathcal{S}_1$) since the discrete time n.

The key point to implement BPF, therefore, is to design a proposal birth density $\beta(\mathbf{x}_{n|n-1}|\mathbf{z}_{1:n-1})$ and another proposal survival density $\xi(\mathbf{x}_{n|n-1}|\mathbf{x}^{(i)}_{1:n-1}, \mathbf{z}_{1:n-1})$.

a) Proposal survival-density: In practice, the proposal survival density may be simplified. Based on the predicted particle weights $\{w^{(i)}_{n-1|n-2}\}$, the posterior density of the $(n-1)$th time is firstly approximated, i.e.,

$$\hat{w}^{(i)}_{n-1|n-1} \propto \varphi_n\left(\mathbf{z}_{n-1}\left|\boldsymbol{\mathcal{F}}^{(i)}_{n-1|n-2}\right.\right) \times \hat{w}^{(i)}_{n-1|n-2}. \tag{40}$$

Secondly, total $I-B$ discrete particles will be drawn from $\sum_{i=1}^{I} w^{(i)}_{n-1|n-1}\delta(\mathbf{x}-\mathbf{x}^{(i)}_{n-1|n-1})$. The updated particles of time $n-1$ will survive and, furthermore, are reserved for subsequent time n directly [29].

b) Proposal birth-density: As a PU may turn off randomly in CR scenarios, there are two practical challenges inhering in the design of the proposal birth density. First, the proposal birth density of the nth discrete time, which is assumed to be identical to the *a priori* birth density, i.e., $\beta(\mathbf{x}_{n|n-1}|\mathbf{z}_{1:n-1}) = b_{n|n-1}(\mathbf{x}_{n|n-1})$, will be relevant to the PU's emission state of the last time $(n-1)$, i.e., $s_{n-1} \in S$. This is easy to follow, i.e., compared with the situation $s_{n-1} = S_1$, the uncertainty in estimating the nth PU's position (i.e. $\mathbf{l}_n$) may be enlarged under $s_{n-1} = S_0$. Second, such an uncertainty of PU's locations will even vary along time, i.e., changing with the lasting length of PU's silence state S_0. In practice, the above difficulties, if left unchecked, may easily lead to the mistracking of PU's positions in the considered spectrum-location awareness scenarios.

To deal with realistic challenges above and avoid the mistracking of moving locations when a PU readily turns off, a promising adaptive horizon expanding (AHE) mechanism is particularly designed, by taking the uncertainty adaptation into full account. For simplicity, the lasting length of $s_{n-1} = S_0$ is denoted by J, i.e., $s_{n-j} = S_0$ for $0 < j < J$ and $s_{n-J-1} = S_1$. The basic idea behind our designed AHE is that the uncertainty of the proposal birth density would be *accumulated* as the lasting length J increases, as illustrated by Fig. 2. Within the new AHE framework, PU's positions may be tracked via the following two criterions.

1) After the PU enters into H_0 at time $(n-J)$, the predictive position estimations in subsequent time slots (i.e., $n-J+1, n-J+2, \cdots, n-1$) will be derived based on the previously estimated PU's speed and orientation, as shown by the Fig. 2.
2) Once the PU re-emits at time n, then its dynamic positions will be estimated by fully utilizing the likelihood information. Correspondingly, in this situation, the birth density of the discrete time n will be specified by:

$$b_{n|n-1}(\mathbf{x}_{n|n-1}) \sim f_v(v_n|J) \times f_\theta(\theta_n|J), \tag{41}$$

where the two independent 1-D densities, i.e., the speed density $f_v(v_n|J)$ and the orientation density $f_\theta(\theta_n|J)$ which are updated adaptively according to spectrum sensing results (i.e., $s_{1:n-1}$), will jointly specify a 2-D prior density of PU's locations. It is supposed that, as the lasting length J of S_0 increases, the cover area of this birth density would be also expanded so as to track the PU positions even after a long time of silence. In practice, these two adaptive densities will be specified as:

$$f_v(v_n|J) = \frac{1}{\sigma_v\sqrt{2\pi J}} exp\left[-\frac{(v_n - J\hat{v}_{n-J-1})^2}{2J\sigma_v^2}\right], \tag{42}$$

$$f_\theta(\theta_n|J) = \frac{1}{2J\sigma_\theta^2} exp\left(-\frac{|\theta_n - J\hat{\theta}_{n-J-1}|}{J\sigma_\theta^2}\right), \tag{43}$$

respectively, where the term $\hat{v}_{n-J-1}$ and $\hat{\theta}_{n-J-1}$ denote the estimated PU's speed and orientation of the $(n-J-1)$th time, which may be either derived from an instantaneous estimation based on the $(n-J-2)$th and the $(n-J-1)$th time, or the G-average estimation, e.g., from the $(n-J-G)$th time to the $(n-J-1)$th time.

In the analysis, we employ the simple instantaneous estimation, i.e.,

$$\hat{v}_{n-J-1} = \|\hat{\mathbf{l}}_{n-J-1} - \hat{\mathbf{l}}_{n-J-2}\|_2, \tag{44}$$
$$\hat{\theta}_{n-J-1} = \mathtt{ang}(\hat{\mathbf{l}}_{n-J-1} - \hat{\mathbf{l}}_{n-J-2}), \tag{45}$$

Note that, after a PU enters into the emission state, then the uncertainty of the birth density will be reduced gradually.

Based on the designed survival-density and birth-density, we may now draw discrete particles from one unified proposal distribution $\xi_{n|n-1}(\mathbf{x}_{n|n-1}|\mathbf{x}^{(i)}_{1:n-1}, \mathbf{z}_{0:n})$, i.e.,

$$\mathbf{x}^{(i)}_{n|n-1} \sim \xi_{n|n-1}\left(\mathbf{x}_{n|n-1}\left|\mathbf{x}^{(i)}_{1:n-1}, \mathbf{z}_{0:n-1}\right.\right), \quad i = 1, 2, \cdots, I-B, I-B+1, \cdots, I. \tag{46}$$

With the suggested survival and birth densities, the Bayesian inference will now be numerically realized. Relying on a group of new simulated particles $\mathbf{x}^{(i)}_{n|n-1}$ and the probability weights $w^{(i)}_{n|n-1}$ calculated from (43), the intractable integration on $f_{n|n-1}(\mathbf{x})$ will be replaced by summations, i.e.,

$$\int r_n(\mathbf{z}_n|\mathbf{x}) f_{n|n-1}(\mathbf{x}) d\mathbf{x} \backsimeq \sum_{i=1}^{I} r_n\left(\mathbf{z}_n\left|\mathbf{x}^{(i)}_{n|n-1}\right.\right) w^{(i)}_{n|n-1}. \tag{47}$$

Based on eq. (36), the term $f_{n|n}(\mathbf{x})$ will be approximated. So, PU's dynamic locations will be estimated via:

$$\hat{\mathbf{l}}_n = \arg \max_{\mathbf{x}_n \in \mathbb{R}^2} \tilde{f}_{n|n}(\mathbf{x}_n), \tag{48}$$

where the *a posteriori* probability is approximated by:

$$\tilde{f}_{n|n}(\mathbf{x} \to \mathbf{x}(j)) = \sum\nolimits_{i \in \mathcal{X}_j} w^{(i)}_{n|n} \Big/ \sum_{i=1}^{I} w^{(i)}_{n|n}, \quad \mathcal{X}_j = \left\{ i \left| \mathbf{x}^{(i)}_{n|n} = \mathbf{x}(j) \right. \right\}. \tag{49}$$

The unknown PU state is finally derived by comparing the posterior existence density with a predefined threshold χ, i.e.,

$$\hat{\lambda}_n = \begin{cases} 1 & \text{if } q_{n|n} \geq \chi, \quad (50a) \\ 0 & \text{if } q_{n|n} < \chi. \quad (50b) \end{cases}$$

where χ is configured to $\chi = 0.5$ under a Bayesian criterion.

c) Algorithm flow: To sum up, two main parts are involved by the designed spectrum-location awareness algorithm, as illustrated by Fig. 3. (1) Based on the recursive *predict-update* propagation and by utilizing observation trajectory $\mathbf{z}_{1:n}$, the posterior existence probability $q_{n|n}$ and the spatial PDF $f_{n|n}(\mathbf{x})$ are estimated. (2) In the case of $q_{n|n} < \chi$, the designed AHE will be applied and, with the help of BPF, the unknown emission state of PU will be detected and its locations will be estimated jointly.

It is noted one counter, namely J, is used to record the degrees of the prior uncertainty after a PU enters into the silence state (i.e., H_0), which is of practical use to the designed AHE process. It will be clamped to 1 every time the PU transiting to the emission state (i.e., H_1). Otherwise, if the PU have resided in H_0 for one sensing period T_S, then J will be updated by $J = J + 1$.

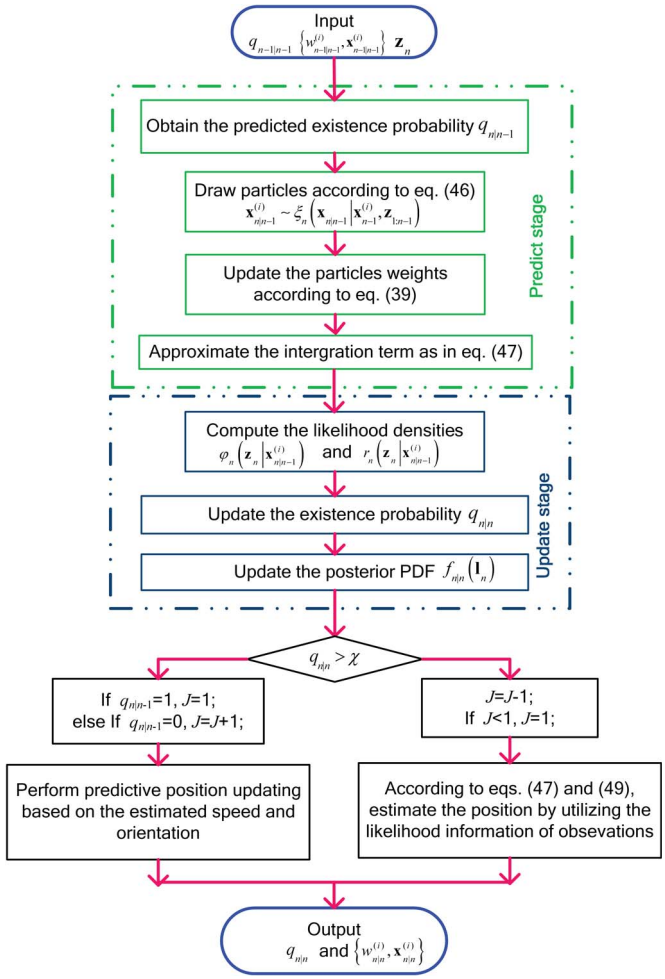

Fig. 3. Schematic flow of the DS algorithm implemented by BPF.

d) Implementations: Firstly, although the PU-SU distance $d_{n,k}$ is involved in observations, it will not be estimated directly by BPF. With the probable PU's locations (or a group of simulated particles) and K observations, the distance $d_{n,k}$ will be evaluated implicitly by the data center, as the position of each deployed SU is known as *a priori*.

Secondly, it should be noteworthy that, given the *phase-free* RSS observations $z_{n,k}$, the generalization to other modulated signals is also straightforward [26]. From the algorithm derivations, the proposed scheme relies essentially on the dynamic model and the related likelihoods of observations. Once the likelihoods of various signals are available, it will be ready for either single carrier (SC) or orthogonal frequency-division multiplexing (OFDM) signals, even without *a priori* modulation formats. One may refer to the previous works [26], [34], in which the likelihoods (i.e., phase-free observations) of unknown modulated signals have been derived.

e) Complexity: Based on the elaborations above, we may further analyze the complexity which is roughly measured by the total numbers of multiplication operations. Firstly, to obtain RSS observations, $\mathcal{O}(M)$ multiplications are required in each SU node. Secondly, for the implementing of BPF process, the computation complexity may become proportional to the size of simulated particles, i.e., I. Thus, the total complexity of this designed DS algorithm is measured by $\mathcal{O}(MK + I)$.

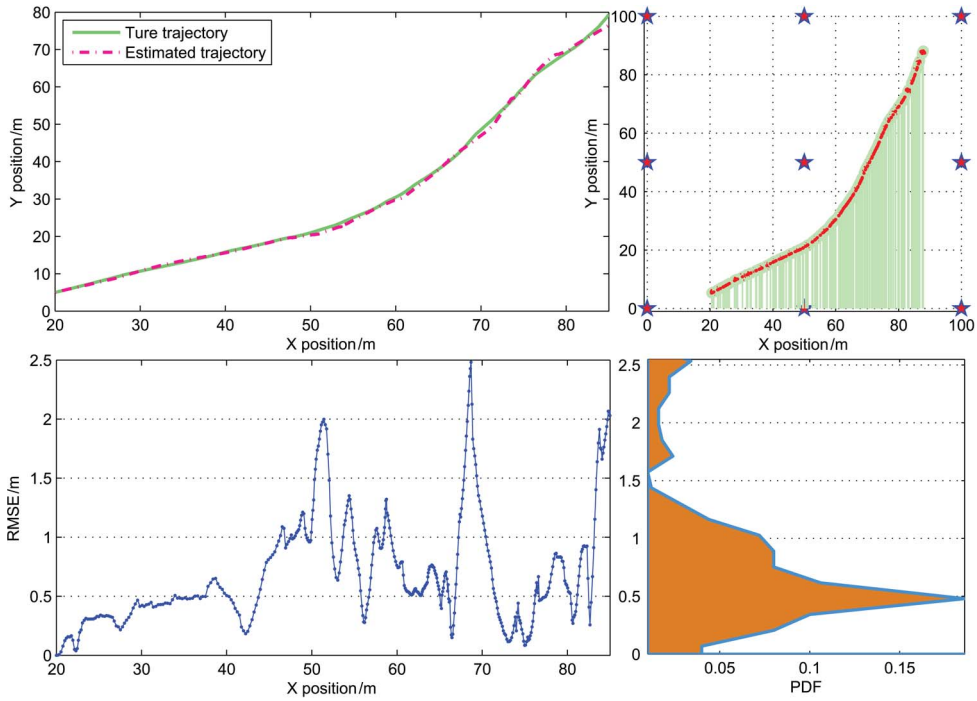

Fig. 4. (a) The *top-left* figure gives the true trajectory and the estimated trajectory of the proposed DS scheme. Here, the sampling length is $M = 200$ and SNR is configured to 10 dB. (b) The *top-right* figure shows the prior positions of $K = 9$ collaborative SU nodes, which are located at the vertexes of a 2-D grid. Notice that, these stems sign PU's emission states along the moving trajectory. (c) The *below-left* figure plots the RMSE of the estimated trajectory. (d) The *below-right* figure plots the statistic distribution of RMSE values.

IV. Numerical Simulations

In this section, the performances of both spectrum sensing and PU's localization accuracy will be investigated in realistic spectrum-location awareness applications.

1) Sensing Metric: Since a Bayesian approach is used by the proposed scheme, the total detection probability is adopted as a metric for sensing performance as in [27], [33], i.e.,

$$P_D \triangleq 1 - p(H_1)P_m - p(H_0)P_f. \tag{51}$$

Here, the false alarm $P_f \triangleq \Pr(H_1|H_0)$ measures the spectral utilization, while the missed detection probability $P_m \triangleq \Pr(H_0|H_1)$ controls the interferences from SUs to PU which is aroused by miss detections. Such a performance metric remains quite different from the classical NP criterion, in which a main objective is either to minimize P_m for a target P_f, or to minimize the P_f for a target P_m. It is noted that, as the major merit of this new metric, the spectral utilization to unused bands and the potential interference to PUs can be jointly taken into accounts.

2) Localization Metric: For the dynamic tracking of PU's locations, as a common performance metric, the root mean square error (RMSE) of estimated positions will be adopted, i.e.,

$$RMSE \triangleq \mathsf{E}\left\{\frac{1}{N}\sqrt{\sum_{n=1}^{N}\|\hat{\mathbf{l}}_n - \mathbf{l}_n\|_2^2}\right\}. \tag{52}$$

A. Simulation Configurations

In the experiments, K SUs are located on the vertexes of a 2-D grid, while a PU is moving onto this grid with its emission states switching randomly. Such a realistic scenario may correspond to the indoor office or an outdoor square, where several anchor SU nodes are deployed on the borders. In the simulation, the border length of the grid is set to 100 m. For the case of $K = 4$, four SU nodes are located at (0, 0), (0, 100), (100, 0), (100, 100). For another case of $K = 9$, then SU nodes are located at (0, 0), (0, 50), (0, 100), (50, 0), (100, 0), (50, 100), (100, 50), (50, 50), (100, 100), as illustrated by the top-right of Fig. 4. Both the initial speed $v_0 = 0.2$ m/s and the initial orientation $\theta_0 = 0.5$ rad are assumed to be known by the data center. Without loss generality, the driven variance of PU's speed is configured to $\sigma_v^2 = 0.0002$, while that of its orientation is $\sigma_\theta^2 = 0.02$. The survival probability p_s and the birth probability p_b are both configured to 0.5. During the experiments, the average SNR of K SUs is obtained from total N time slots, given the Gaussian noise variance σ_w^2, i.e., $SNR \triangleq \frac{1}{NK}\sum_{k=1}^{K}\sum_{n=0}^{N-1}\frac{\gamma_k^2 E_s p_s}{d_{k,n}^{\alpha}\sigma_w^2}$. Here, without losing generality, K receiving gains γ_k $(k = 1, 2, \cdots, K)$ are all configured to 1, and the path-loss constant is set to $\alpha = 2.2$. It is seen from Fig. 4 that, when a relatively high SNR is provided (e.g., >10 dB), the time-varying trajectory of the moving PU would be estimated with a high accuracy when the number of SUs is $K = 9$. From numerical results shown by the below-right figure, although the maximum RMSE is 2.49, the ratio of RMSE exceeding 1.5 remains less than 10%.

B. Is Location Necessary?

In the first experiment, the influence from PU's moving positions on the spectrum sensing is investigated. The number of SUs is still set to $K = 4$ and the sample size is $M = 100$; the size of simulated particles are configured to $I = 1000$, while

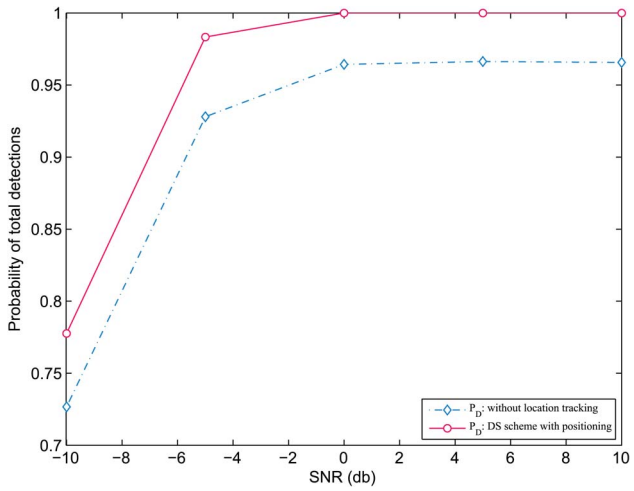

Fig. 5. Spectrum sensing performances of the DS algorithm and the tradition sensing scheme. In the simulation, K is configured to 4, M is 100 and (p_b, p_s) is set to (0.5, 0.5).

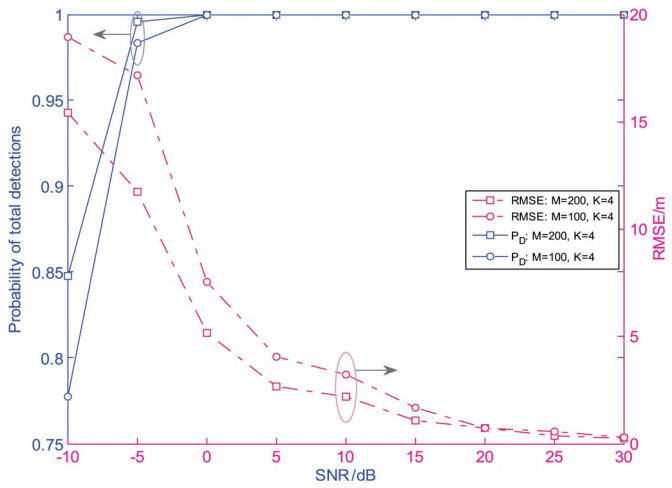

Fig. 6. The sensing and positions estimation performance of the DS algorithm under different M. In the simulation, K is configured to 4, (p_b, p_s) is set to (0.5, 0.5).

the number of birth particles is $B = 500$. Each curve is derived numerically based on 10 independent realizations. For the traditional ED scheme, it is assumed the accurate trajectory of a moving PU remains unknown. The average receiving power, instead, is assumed as *a priori* in each SU. In the data center, the cooperative sensing scheme is used.

As shown by Fig. 5, the *SNR wall* will be appeared in traditional schemes without a real-time tracking of PU's moving positions. The probability of total detections P_D will become converged to 0.962, no matter what SNR is provided. This SNR wall is attributed primarily to the reception *uncertainty* aroused by PU's unknown locations. Recall that the energy observation is inversely proportional to the power of distance, i.e., $z_{n,k} \propto \frac{1}{d_{n,k}^2}$. Even if an active PU is moving around, the energy observation in SUs will be changed dramatically due to the resulting *far-and-near* effect. In absence of its accurate positions, the missing detections will easily occurs when a PU emitting signals moves far away from the SUs. In comparison, if the PU's locations are acquired jointly, the interrupted influence from the far-and-near effects may be calibrated when making a decision on the existence of PU. So, the uncertainty introduced by a PU's mobility will be removed and, as a consequence, the performance of the new DS scheme can be promoted by eliminating the SNR wall.

The benefits of the PU's localization information are not only the enhanced sensing performance, but also more flexible strategies of accessing primary bands. That is, if the accurate PU's position is perceived by SUs, then beam-forming techniques, e.g., the simple beam switching in [35], can be adopted to conduct CR transmissions even an active PU is *nearby*. This indicates a full two-dimensional *time-spatial* usage of primary bands and, therefore, the spectral efficiency will be improved significantly with the PU's localization information.

C. Sampling Length M

In the second experiment, the effects from different sampling size M are investigated. Each curve is also derived numerically

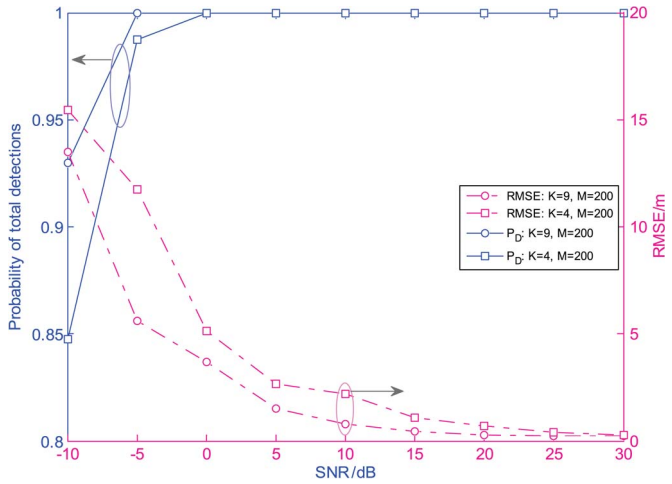

Fig. 7. The sensing and positions estimation performance of the DS algorithm under different number of SUs. In the simulation, the sample size M is configured to 200, (p_b, p_s) is set to (0.5, 0.5).

based on 10 independent realizations. In our simulation, the number of SUs is set to $K = 4$, the size of simulated particles are configured to $I = 1000$, while the number of birth particles is $B = 500$.

It is shown from Fig. 6 that, in practice, M will affect the sensing performance. To be specific, the larger the sample size M, the better the sensing performance. A rough detection gain of 2 dB will be achieved by increasing the sampling size M from 100 to 200. With multiple collaborative SU nodes, the probability of total detections P_D may achieve 1 when SNR surpass 0 dB and $M = 100$. The RMSE curves of different M are plotted together in Fig. 6. It is observed that the RMSE will also be reduced by increasing M. For example, an estimation gain of 3∼5 dB may be achieved via increasing M from 100 to 200. Thus, the localization accuracy may be promoted effectively by adopting a larger M in low SNRs, but at the expense of a prolonged sensing time. Notice that, in high SNR regions (e.g., SNR > 15 dB), the improvement on localizations, nevertheless, may become limited when increasing M.

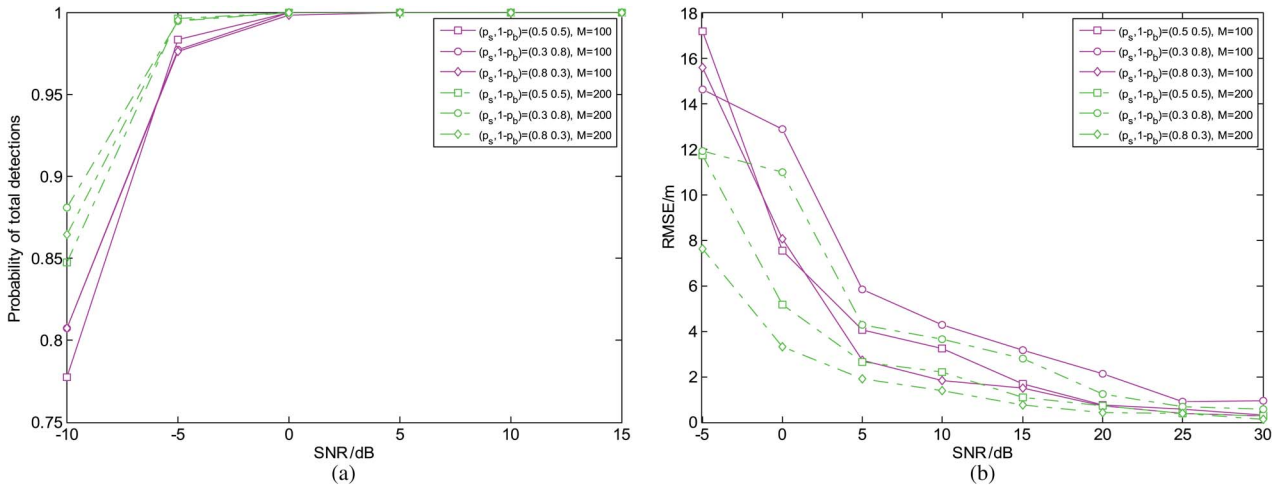

Fig. 8. Joint sensing and location performances of the proposed DS algorithm under different (p_b, p_s). In the simulation, K is configured to 4. (a) The probability of total detections, i.e., P_D; and (b) the RMSE performance.

D. Number of SUs

In the third experiment, both the sensing and localization performance of the new DS scheme is investigated under different numbers of SUs (i.e., K). The sample size is set to $M = 200$. Two kinds of collaborative SUs are compared, i.e., $K = 4$ and 9. From Fig. 7, if K increases from 4 to 9, then an estimation gain of 2 dB may be obtained. A very similar trend may be observed to the RMSE curves. To be specific, when K increases from 4 to 9, the RMSE value may decrease from 2.188 to 0.784, when the SNR is configured to 10 dB. Thus, increasing the number of collaborative SUs is usually an effective approach to enhance the performances of both spectrum sensing and PU localization. As a practical compromise, however more SUs will lead to higher computational complexity and deployment cost.

E. PU's Dynamic Property

Since the tracking of PU's moving positions relies essentially on the RSS acquired from its emission signals, the dynamic transitional property of PU may also affect the performances of joint estimations. In this numerical experiment, the number of collaborative SUs is $K = 4$. It is seen from Fig. 8 that, although the spectrum sensing may not be remarkably affected by PU's dynamic behaviors, the localization accuracy will be influenced noticeably. To be specific, the larger the duration ratio between PU's emission state (i.e., S_1) and silence state (i.e., S_0), the more promising the localization performance. From Fig. 8(b), compared with a shorter PU's emission duration (e.g., $p_s = 0.3$, $1 - p_b = 0.8$), the RMSE will be remarkably reduced from 4.27 to 1.84 when a longer emission duration (e.g., $p_s = 0.8$, $1 - p_b = 0.3$) is considered, if the sampling size is configured to $M = 100$ and SNR=10 dB. This is also easy to understand, i.e., the tracking of PU's locations may become more accurate premised on more useful RSS information. Thus, despite a lower chance of the spectral reuse when the moving PU staying more time in the emission state, a more promising localization performance will be obtained. As a consequence, another dimension spatial reuse may be reinforced based on the accurately estimated PU's locations.

F. Practical Considerations

When the proposed DS scheme with joint location tracking is applied to future 5G communications, some other practical aspects should be taken into considerations.

1) Tradition positioning techniques can be premised on ToA, time difference of arrival (TDoA), angle of arrival (AoA), RSS or the hybrid information [36]. For the location tracking of LTE-A or 3GPP-LTE, TDoA has been widely recommended [37]–[40], as a compromise between the implementation cost (e.g., excluding both the precise synchronization as in ToA and the placement of multi-antenna as in AoA) and the localization performance. For the considered spectrum and location awareness scenarios, the RSS information, as mentioned, suits better due to the absence of cooperation between PU and SUs. In real CRs, the synchronization sequence (e.g., the positioning reference signal required by TDoA) between a base station and mobile users are usually unavailable. As far as the practical deployments are concerned, therefore, the suggested RSS-based scheme seems to be more widely applicable.
2) To sum up, the existing localization schemes for LTE/LTE-A may be grouped into three categories [36], i.e., Cell-ID based approach [38], the least square (LS) scheme [37] and the PF scheme [39], [40]. With regards to the implementation complexity, the Cell-ID method is no-doubt the simplest, which has a constant complexity $\mathcal{O}(1)$ by directly acquiring the ID number [38]. Another commonly used LS scheme has a moderate complexity

of $\mathcal{O}(3K^3 + K^2)$, and the PF method is more complicated with a complexity of $\mathcal{O}(I)$, i.e., it usually meets $I \gg K^3$ [4]. When it comes to the tracking accuracy, the average RMSE of a Cell-ID method is typically around 20∼30 m [38], [40], and that of LS schemes is about 10∼20 m [37], [39]. The PF scheme may obtain the most favorable tracking RMSE, about 5∼15 m [39], [40]. For the proposed DS algorithm, the complexity and tracking performance will be comparable to the existing PF schemes. For example, other than the acquisition of RSS information, the computational complexity of the BPF process (at the date center) is also $\mathcal{O}(I)$. When the measured SNR is -5 dB, the average RMSE in heterogeneous LTE-A applications may approach 13 m (with TDoA information) [40], while the average RMSE of this proposed scheme is about 16 m. It is noteworthy that, in our new scheme, however the more general RSS information is assumed and, furthermore, the more challenging joint detection and estimation scenario (i.e., with a mixed objective of sensing the PU's dynamical state and tracking its positions) is considered.

V. Conclusion

A new DS paradigm is proposed to realize spectrum sensing and joint PU's location tracking in future mobile spectrum-sharing applications. A general DSM is firstly established to thoroughly characterize dynamic behaviors of both unknown PU's states and its moving locations. Relying on the RFS, a flexible estimation algorithm is developed, which tracks PU's moving positions blindly at the same time of detecting its random emission states. To overcome the mis-tracking of PU in realistic CR scenarios, which may be easily aroused by the intermittent disappearances of PU's emission signals (or RSS information), a promising AHE scheme is designed by updating the prior uncertainty of location estimations adaptively. The DS scheme is finally implemented via an SIS-based Bernoulli PF mechanism, by numerically approximating the analytically intractable posterior density. Experiments validate the proposed DS scheme. By taking mutual interrelations between sensing and dynamic localization into full accounts, it is shown that the PU's unknown emission states can be detected effectively even in the presence of a moving PU. Moreover, the estimated PU's real-time locations, as an extra benefit of sensing process, may be utilized to improve network performances, by exploiting both spectral and spatial resource in DSA scenarios. The more challenging time-varying fading channels will be investigated in the future work. The new DSM and DS scheme, which may be further extended to other scenarios, provide a brand-new idea for further spectrum and location awareness 5G communications.

Acknowledgment

We greatly thank the anonymous reviewers for their constructive comments that allowed us to improve the paper significantly.

References

[1] J. G. Andrews *et al.*, "What will 5G be?" *IEEE J. Sel. Areas Commun.*, vol. 32, no. 6, pp. 1065–1082, Jun. 2014.
[2] E. Axell, G. Leus, E. G. Larsson, and H. V. Poor, "Spectrum sensing for cognitive radio: State-of-the-art and recent advances," *IEEE Signal Process. Mag.*, vol. 29, no. 3, pp. 101–116, May 2012.
[3] Y. C. Liang, K. C. Chen, G. Y. Li, and P. Mahonen, "Cognitive radio networking and communications: An overview," *IEEE Trans. Veh. Technol.*, vol. 60, no. 7, pp. 3386–3407, Sep. 2011.
[4] S. Haykin, "Cognitive radio: Brain-empowered wireless communications," *IEEE J. Sel. Areas Commun.*, vol. 23, no. 2, pp. 201–220, Feb. 2005.
[5] J. Ma, G. Y. Li, and B. H. Juang, "Signal processing in cognitive radio," *Proc. IEEE*, vol. 97, no. 5, pp. 805–823, May 2009.
[6] L. Lu, X. W. Zhou, U. Onunkwo, and G. Y. Li, "Ten years of cognitive radio technology," *EURASIP J. Wireless Commun. Netw.*, vol. 28, no. 1, p. 214, 2012.
[7] L. Yang and P. P. Wang, "Location based autonomous power control for ICIC in LTE-A heterogeneous networks," in *Proc. IEEE GLOBECOM*, Houston, TX, USA, Dec. 2011, pp. 1–6.
[8] H. Celebi and H. Arslan, "Utilization of location information in cognitive wireless networks," *IEEE Wireless Commun.*, vol. 14, no. 4, pp. 6–13, Aug. 2007.
[9] F. Y. Li, B. Bai, J. Zhang, and K. B. Letaief, "Location-based joint relay selection and channel allocation for cognitive radio networks," in *Proc. GLOBECOM*, Houston, TX, USA, Dec. 5–9, 2011, pp. 1–5.
[10] F. F. Digham, M. S. Alouini and M. K. Simon, "On the energy detection of unknown signals over fading channels," in *Proc. IEEE ICC*, Anchorage, AK, USA, May 2003, vol. 5, pp. 3575–3579.
[11] H. S. Chen, W. Gao, and D. G. Daut, "Signature based spectrum sensing algorithms for IEEE 802.22 WRAN," in *Proc. IEEE ICC*, Glasgow, U.K., Jun. 2007, pp. 6487–6492.
[12] P. D. Sutton, K. E. Nolan, and L. E. Doyle, "Cyclostationary signature in practical cognitive radio applications," *IEEE J. Sel. Areas Commun.*, vol. 26, no. 1, pp. 13–24, Jan. 2008.
[13] Z. Tian and G. B. Giannakis, "A wavelet approach to wideband spectrum sensing for cognitive radios," in *Proc. IEEE CROWNCOM*, Mykonos Island, Greece, Jun. 2006, pp. 1–5.
[14] Z. Tian and G. B. Giannakis, "Compressed sensing for wideband cognitive radios," in *Proc. IEEE ICASSP*, Honolulu, HI, USA, Apr. 2007, pp. 1357–1360.
[15] Y. H. Zeng and Y. C. Liang, "Eigenvalue-based spectrum sensing algorithms for cognitive radio," *IEEE Trans. Commun.*, vol. 57, no. 6, pp. 1784–1793, Jun. 2009.
[16] J. Ma and Y. Li, "A probability-based spectrum sensing scheme for cognitive radio," in *Proc. IEEE ICC*, Beijing, China, May 2008, pp. 3416–3420.
[17] *Draft Standard for Wireless Regional Area Networks Part 22: Cognitive Wireless RAN Medium Access Control (MAC) and Physical Layer (PHY) Specifications: Policies and Procedures for Operation in the TV Bands*, IEEE P802.22/D1.0, Apr. 2008.
[18] I. Guvenc and C. C. Chong, "A survey on TOA based wireless localization and NLOS mitigation techniques," *IEEE Commun. Surveys Tuts.*, vol. 3, no. 11, pp. 107–124, 3rd Quart. 2009.
[19] L. Taponecco, A. A. Damico, and U. Mengali, "Joint TOA and AOA estimation for UWB localization applications," *IEEE Trans. Wireless Commun.*, vol. 10, no. 7, pp. 2207–2217, Jul. 2011.
[20] M. Kazemi, B. Mahboobi, and M. Ardebilipour, "Performance analysis of simultaneous location and power estimation using WLS method for cognitive radio," *IEEE Commun. Lett.*, vol. 15, no. 10, pp. 1062–1064, Oct. 2011.
[21] H. Celebi and H. Aralan, "Cognitive positioning systems," *IEEE Trans. Wireless Commun.*, vol. 12, no. 6, pp. 4475–4483, Dec. 2007.
[22] T. Xue, Y. Shi, and X. D. Dong, "A framework for location-aware strategies in cognitive radio systems," *IEEE Wireless Commun. Lett.*, vol. 1. no. 1, pp. 30–33, Feb. 2012.
[23] J. Wang, J. H. Chen, and D. Cabric, "Cramer–Rao bounds for joint RSS/DOA-based primary user localization in cognitive radio networks," *IEEE Trans. Wireless Commun.*, vol. 12, no. 3, pp. 1363–1375, Mar. 2013.
[24] A. W. Min and K. G. Shin, "Robust tracking of small-scale mobile primary user in cognitive radio networks," *IEEE Trans. Parallel Distrib. Syst.*, vol. 24, no. 4, pp. 778–788, Apr. 2013.
[25] Y. C. Liang, Y. H. Zeng, E. C. Y. Peh, and T. H. Anh, "Sensing-throughput tradeoff for cognitive radio networks," *IEEE Trans. Wireless Commun.*, vol. 7, no. 4, pp. 1326–1337, Apr. 2008.

[26] B. Li, C. L. Zhao, M. W. Sun, and A. Nallanathan, "Spectrum sensing for cognitive radios in time-variant flat fading channels: A joint estimation approach," *IEEE Trans. Commun.*., vol. 62, no. 8, pp. 665–2680, Aug. 2014.
[27] B. Li, Z. Zhou, and A. Nallanathan, "Joint estimation based spectrum sensing for cognitive radios in time variant flat fading channel," in *Proc. IEEE GLOBECOM*, Atlanta, GA, USA. Dec. 2013, pp. 3212–3217.
[28] R. Mahler, *Statistical Multisource Multitarget Information Fusion*. Norwood, MA, USA: Artech House, 2007.
[29] B. T. Vo and B. N. Vo, "A random finite set conjugate prior and application to multi-target tracking," in *Proc. 7th IEEE ISSNIP*, Adelaide, Australia, Dec. 2011, pp. 431–436.
[30] B. T. Vo, B. N. Vo, and A. Cantoni, "Bayesian filtering with random finite set observations," *IEEE Trans. Signal Process.*, vol. 56, no. 4, pp. 1313–1326, Apr. 2008.
[31] B. Ristic, B. T. Vo, B. N. Vo, and A. Farina, "A tutorial on bernoulli filters: Theory, implementation and applications," *IEEE Trans. Signal Process.*, vol. 61, no. 13, pp. 3406–3430, Jul. 2013.
[32] P. M. Djuric *et al.*, "Particle filtering," *IEEE Signal Process. Mag.*, vol. 20, no. 5, pp. 19–38, Sep. 2003.
[33] W. Zhang, R. K. Mallik, and K. B. Letaief, "Cooperative spectrum sensing optimization in cognitive radio networks," in *Proc. IEEE ICC*, Beijing, China, May 19–23, 2008, pp. 3411–3415.
[34] B. Li, M. W. Sun, C. L. Zhao, and A. Nallanathan, "Energy detection based spectrum sensing for cognitive radios over time-frequency doubly selective fading channels," *IEEE Trans. Signal Process.*, vol. 63, no. 2, pp. 402–417, Jan. 2015.
[35] B. Li, Z. Zhou, W. X. Zou, X. B. Sun, and G. L. Du, "On the efficient beam-forming training for 60 ghz wireless personal area networks," *IEEE Trans. Wireless Commun.*, vol. 12, no. 2, Feb. 2013, pp. 504–515.
[36] S. S. Cherian and A. N. Rudrapatna, "LTE location technologies and delivery solutions," *Bell Labs Tech. J.*, vol. 18, no. 2, pp. 175–194, Sep. 2013.
[37] S. Frattasi, M. Monti, and R. Prasad, "Cooperative mobile user location for next-generation wireless cellular networks," in *Proc. IEEE ICC*, Istanbul, Turkey, Jun. 11–15, 2006, pp. 5760–5765.
[38] M. A. Amin and S. Fischer, "Position location of LTE femtocells deployed in a cluster," in *Proc. ICL-GNSS*, Starnberg, Germany, Jun. 25–27, 2007, pp. 1–6.
[39] C. Gentner, E. Munoz, M. Khider, and E. Staudinger, "Particle filter based positioning with 3GPP-LTE in indoor environments," in *Proc. IEEE/ION PLANS*, Myrtle Beach, SC, USA, Apr. 23–26, 2012, pp. 301–308.
[40] K. T. Lee, P. H. Tseng, C. H. Chen, and K. T. Feng, "Femto-assisted location estimation in macro/femto heterogeneous networks," in *Proc. IEEE WCNC*, Shanghai, China, Apr. 7–10, 2013, pp. 2305–2310.

Bin Li received the Bachelor's degree in electrical information engineering from Beijing University of Chemical Technology (BUCT), Beijing, China, in 2007 and the Ph.D. degree in communication and information engineering from Beijing University of Posts and Telecommunications (BUPT), in 2013. He joined BUPT in 2013, as a Lecturer with the School of Information and Communication Engineering (SCIE). His current research interests are focused on statistical signal processing algorithms for wireless communications, e.g., ultra-wideband (UWB), wireless sensor networks, millimeter-wave (mm-Wave) communications and cognitive radios (CRs). He has published more than 60 journal and conference papers. He received the 2011 ChinaCom Best Paper Award, and the 2010 and 2011 BUPT Excellent Ph.D Student Award Foundation. He served as the regular reviewer for IEEE TRANSACTIONS ON COMMUNICATIONS, IEEE TRANSACTIONS ON SIGNAL PROCESSING and IEEE TRANSACTIONS ON WIRELESS COMMUNICATIONS.

Shenghong Li received the B.S. and the M.S. degrees in electrical engineering from Jilin University of Technology, Changchun, China, in 1993 and 1996, respectively, and the Ph.D. degree in radio engineering from Beijing University of Posts and Telecommunications (BUPT), Beijing, China, in 1999. Since 1999, he has been as Research Fellow, Associate Professor and Professor, successively, at Shanghai Jiao Tong University (SJTU), China. In 2010, he was a Visiting Scholar at Nanyang Technological University, Singapore. His research interests include information security, signal and information processing, cognitive radio networks, artificial intelligence.

He has published more than 80 papers, co-authored four books, and holds ten granted patents. In 2003, he received the 1st Prize of Shanghai Science and Technology Progress in China. In 2006 and 2007, he was elected for New Century Talent of Chinese Education Ministry and Shanghai Dawn Scholar.

Arumugam Nallanathan (S'97–M'00–SM'05) is a Professor of Wireless Communications in the Department of Informatics, King's College London (University of London). He served as the Head of Graduate Studies in the School of Natural and Mathematical Sciences, King's College London, in 2011 and 2012. He was an Assistant Professor in the Department of Electrical and Computer Engineering, National University of Singapore from August 2000 to December 2007. His research interests include 5G Technologies, millimeter wave communications, cognitive radio and relay networks. In these areas, he has co-authored nearly 250 papers. He is a co-recipient of the Best Paper Award presented at the 2007 IEEE International Conference on Ultra-Wideband (ICUWB2007). He is a Distinguished Lecturer of IEEE Vehicular Technology Society.

He is an Editor for IEEE TRANSACTIONS ON COMMUNICATIONS and IEEE TRANSACTIONS ON VEHICULAR TECHNOLOGY. He was an Editor for IEEE TRANSACTIONS ON WIRELESS COMMUNICATIONS (2006–2011), IEEE WIRELESS COMMUNICATIONS LETTERS and IEEE SIGNAL PROCESSING LETTERS. He served as the Chair for the Signal Processing and Communication Electronics Technical Committee of IEEE Communications Society, Technical Program Co-Chair (MAC track) for IEEE WCNC 2014, Co-Chair for the IEEE GLOBECOM 2013 (Communications Theory Symposium), Co-Chair for the IEEE ICC 2012 (Signal Processing for Communications Symposium), Co-Chair for the IEEE GLOBECOM 2011 (Signal Processing for Communications Symposium), Technical Program Co-Chair for the IEEE International Conference on UWB 2011 (IEEE ICUWB 2011), Co-Chair for the IEEE ICC 2009 (Wireless Communications Symposium), Co-chair for the IEEE GLOBECOM 2008 (Signal Processing for Communications Symposium) and General Track Chair for IEEE VTC 2008. He received the IEEE Communications Society SPCE outstanding service award 2012 and IEEE Communications Society RCC outstanding service award 2014.

Chenglin Zhao received the Bachelor's degree in radio-technology from Tianjin University in 1986, the master's degree in circuits and systems from Beijing University of Posts and Telecommunications (BUPT), Beijing, China, in 1993, and the Ph.D. degree in communication and information system from Beijing University of Posts and Telecommunications, in 1997. At present, he is a Professor at Beijing University of Posts and Telecommunications, Beijing, China. His research is focused on emerging technologies of short-range wireless communication, cognitive radios, 60 GHz millimeter-wave communications.